# Directional spin wavelets on the sphere

Jason D. McEwen, Boris Leistedt, Martin Büttner, Hiranya V. Peiris, and Yves Wiaux

*Abstract*—We construct a directional spin wavelet framework on the sphere by generalising the scalar scale-discretised wavelet transform to signals of arbitrary spin. The resulting framework is the only wavelet framework defined natively on the sphere that is able to probe the directional intensity of spin signals. Furthermore, directional spin scale-discretised wavelets support the exact synthesis of a signal on the sphere from its wavelet coefficients and satisfy excellent localisation and uncorrelation properties. Consequently, directional spin scale-discretised wavelets are likely to be of use in a wide range of applications and in particular for the analysis of the polarisation of the cosmic microwave background (CMB). We develop new algorithms to compute (scalar and spin) forward and inverse wavelet transforms exactly and efficiently for very large data-sets containing tens of millions of samples on the sphere. By leveraging a novel sampling theorem on the rotation group developed in a companion article, only half as many wavelet coefficients as alternative approaches need be computed, while still capturing the full information content of the signal under analysis. Our implementation of these algorithms is made publicly available.

*Index Terms*—Wavelet transforms, harmonic analysis, sampling, sphere, rotation group.

## I. INTRODUCTION

**W**AVELET transforms on the sphere (*e.g.* [1]–[14]) to analyse scalar signals defined on a spherical domain are finding widespread application. For example, wavelet analyses on the sphere have led to many insightful scientific studies in the fields of planetary science (*e.g.* [15], [16]), geophysics (*e.g.* [17]) and cosmology, in particular for the analysis of the cosmic microwave background (CMB) (*e.g.* [18]–[36]; for a review see [37]), among others.

Discrete wavelet frameworks on the sphere that can support the exact synthesis of signals from their wavelet coefficients in a stable manner have received a great deal of attention recently, including: needlets [6]–[8]; directional scale-discretised wavelets [9]–[11]; and the isotropic undecimated and pyramidal wavelet transforms [14]. All three of these approaches have also been extended to analyse signals defined on the three-dimensional ball formed by augmenting the sphere with the radial line [38]–[41], such as the distribution of galaxies in our Universe [42].

Data acquired on spherical domains come in a variety of different forms, not only scalar but also vector and tensor signals defined on the sphere. Spin functions [43] provide a unifying framework for representing such signals, where spin $s = 0$ functions are scalar, $s = \pm 1$ functions are vector, and higher spin orders correspond to tensor functions. An example of a spin $s = \pm 1$ signal of interest is geomagnetic anomalies over the Earth [44], while an example of a spin $s = \pm 2$ signal is the polarised radiation of the CMB [45]. Motivated largely by the analysis of CMB polarisation, spin wavelet transforms on the sphere have been developed recently [46]–[50], focusing predominantly on the spin $s = \pm 2$ setting.

The isotropic undecimated and pyramidal wavelet transforms on the sphere [14] have been extended to spin $s = \pm 2$ signals [46]. A number of constructions are proposed in [46], settling on a transform constructed by firstly decomposing a spin-2 signal into its parity even and odd components, so-called E- and B-mode signals [45], before performing the scalar wavelet transform of [14]. This construction does not easily generalise to signals of arbitrary spin and is restricted to wavelets that can only probe isotropic signal content. The spin curvelet construction of [46] that supports a directional analysis is built on the twelve base-resolution faces of the HEALPIX [51] pixelisation, as are the scalar curvelets of [46], and as such is not natively defined on the sphere. This approach may lead to (blocking) artefacts [14].

Needlets have also been extended to the analysis of spin functions on the sphere, in a variety of manners [47]–[49]. The standard spin needlet construction [47], [48] is defined by a linear projector onto the space of spin functions. Consequently, the needlet coefficients of spin signals are spin quantities themselves, of the same spin number. Alternatively, the so-called mixed needlet construction [49] results in spin needlet coefficients that are scalar quantities. Both spin needlet constructions satisfy excellent localisation and uncorrelation properties and generalise easily to signals of arbitrary spin number [47]–[49]. However, spin needlet constructions can also only probe isotropic signal content.

A spin wavelet framework on the sphere capable of probing the directional intensity of spin signals does not yet exist. We develop such a framework in this article, generalising directional scale-discretised wavelets [9]–[11] to the analysis of signals on the sphere of arbitrary spin. In related articles, we construct spin ridgelet [52] and curvelet [53] transforms defined natively on the sphere and built on the general spin scale-discretised wavelet framework presented herein. In another recent article [54] we show that directional scale-discretised wavelets satisfy excellent localisation and uncorrelation problems similar to needlets, in both the scalar setting and the spin generalisation presented here.

An overview of our spin scale-discretised wavelet construc-

tion was first presented in [55]. In this article, however, we present a more complete construction, prove a number of important properties of the construction, develop new algorithms to compute the wavelet transform exactly and efficiently, evaluate our implementation of these algorithms, and present an illustrative application. The remainder of this article is structured as follows. Harmonic analysis on the sphere and rotation group is reviewed concisely in Sec. II. The directional spin scale-discretised wavelet framework is derived in Sec. III, while an algorithm to compute the wavelet transform and its inverse exactly and efficiently for very large data-sets is presented and evaluated in Sec. IV. An illustrative application is presented in Sec. V, before concluding remarks are made in Sec. VI.

## II. HARMONIC ANALYSIS ON THE SPHERE & ROTATION GROUP

We concisely review harmonic analysis on the sphere and rotation group in this section, presenting the mathematical preliminaries required throughout the remainder of the article. General spin signals on the sphere are first reviewed, before we specialise to spin-2 signals and highlight alternative representations of practical interest. Signals on the rotation group are then discussed, followed by a description of the rotation of functions on the sphere, expressed in both the spatial and harmonic domains.

### A. Spin signals on the sphere

Square integrable spin functions on the sphere $_sf \in \mathrm{L}^2(\mathbb{S}^2)$, with integer spin $s \in \mathbb{Z}$, are defined by their behaviour under local rotations. By definition, a spin function transforms as [43], [45], [56]

$$_sf'(\omega) = \mathrm{e}^{-\mathrm{i}s\chi}\,_sf(\omega) \tag{1}$$

under a local rotation by $\chi \in [0, 2\pi)$, where the prime denotes the rotated function.[1] It is important to note that the rotation considered here is *not* a global rotation on the sphere but rather a rotation by $\chi$ in the tangent plane centred on the spherical coordinates $\omega = (\theta, \varphi)$, with colatitude $\theta \in [0, \pi]$ and longitude $\varphi \in [0, 2\pi)$.

The spin spherical harmonics $_sY_{\ell m} \in \mathrm{L}^2(\mathbb{S}^2)$ form an orthogonal basis for $\mathrm{L}^2(\mathbb{S}^2)$ spin $s$ functions on the sphere, for natural $\ell \in \mathbb{N}$ and integer $m \in \mathbb{Z}$, $|m| \leq \ell$, $|s| \leq \ell$. We adopt the Condon-Shortley phase convention, such that the conjugate symmetry relation $_sY^*_{\ell m}(\theta, \varphi) = (-1)^{s+m}\,_{-s}Y_{\ell,-m}(\theta, \varphi)$ holds. The orthogonality and completeness relations for the spherical harmonics read $\langle _sY_{\ell m},\ _sY_{\ell' m'}\rangle = \delta_{\ell \ell'}\delta_{mm'}$ and

$$\sum_{\ell=0}^{\infty}\sum_{m=-\ell}^{\ell} {}_sY_{\ell m}(\theta,\varphi)_sY^*_{\ell m}(\theta',\varphi') = \delta(\cos\theta - \cos\theta')\delta(\varphi - \varphi'), \tag{2}$$

respectively [43], [45], [56], where $\delta_{ij}$ is the Kronecker delta symbol and $\delta(\cdot)$ is the Dirac delta function. The inner product of $f, g \in \mathrm{L}^2(\mathbb{S}^2)$ is defined by

$$\langle f,\ g\rangle = \int_{\mathbb{S}^2} \mathrm{d}\Omega(\omega)\, f(\omega)\, g^*(\omega)\,, \tag{3}$$

where $\mathrm{d}\Omega(\theta, \varphi) = \sin\theta\, \mathrm{d}\theta\, \mathrm{d}\varphi$ is the usual invariant measure on the sphere and complex conjugation is denoted by $\cdot^*$.

Spin raising and lowering operators, $\eth$ and $\bar{\eth}$ respectively, increment and decrement the spin order of a spin-$s$ function by unity and are defined by [43], [45], [56]

$$\eth \equiv -\sin^s\theta\left(\frac{\partial}{\partial\theta} + \frac{\mathrm{i}}{\sin\theta}\frac{\partial}{\partial\varphi}\right)\sin^{-s}\theta \tag{4}$$

and

$$\bar{\eth} \equiv -\sin^{-s}\theta\left(\frac{\partial}{\partial\theta} - \frac{\mathrm{i}}{\sin\theta}\frac{\partial}{\partial\varphi}\right)\sin^s\theta\,, \tag{5}$$

respectively. The spin-$s$ spherical harmonics can thus be expressed in terms of the scalar (spin-zero) harmonics through the spin raising and lowering operators by [43], [45], [56]

$$_sY_{\ell m}(\omega) = \left[\frac{(\ell-s)!}{(\ell+s)!}\right]^{1/2}\eth^s Y_{\ell m}(\omega)\,, \tag{6}$$

for $0 \leq s \leq \ell$, and by

$$_sY_{\ell m}(\omega) = (-1)^s\left[\frac{(\ell+s)!}{(\ell-s)!}\right]^{1/2}\bar{\eth}^{-s} Y_{\ell m}(\omega)\,, \tag{7}$$

for $-\ell \leq s \leq 0$, where $Y_{\ell m}$ denote the scalar (spin-zero) spherical harmonics.

Due to the orthogonality and completeness of the spin spherical harmonics, any square integrable spin function on the sphere $_sf \in \mathrm{L}^2(\mathbb{S}^2)$ may be represented by its spherical harmonic expansion

$$_sf(\omega) = \sum_{\ell=0}^{\infty}\sum_{m=-\ell}^{\ell} {}_sf_{\ell m}\,_sY_{\ell m}(\omega)\,, \tag{8}$$

where the spin spherical harmonic coefficients are given by the usual projection onto each basis function: $_sf_{\ell m} = \langle _sf,\ _sY_{\ell m}\rangle$. The conjugate symmetry relation of the spin spherical harmonic coefficients is given by $_sf^*_{\ell m} = (-1)^{s+m}\,_{-s}f_{\ell,-m}$ for a function satisfying $_sf^* = \,_{-s}f$ (which for a spin $s = 0$ function equates to the usual reality condition) and follows directly from the conjugate symmetry of the spin spherical harmonics. Throughout, we consider signals on the sphere band-limited at $L$, that is signals such that $_sf_{\ell m} = 0$, $\forall \ell \geq L$. The spherical harmonic transform can be computed exactly and efficiently for band-limited signals by appealing to sampling theorems on the sphere and fast algorithms [57]–[61].

### B. Spin-2 signals on the sphere

Although we typically consider signals of arbitrary spin throughout, we specialise to spin-2 signals on the sphere in some cases to illustrate connections between scalar and spin-2 wavelet transforms. Moreover, the spin-2 setting is of particular interest for the analysis of linearly polarised radiation. We briefly review spin-2 signals in this context.

---

[1]The sign convention adopted for the argument of the complex exponential differs to the original definition [43] but is identical to the convention used in the context of the polarisation of the CMB [45].

The Stokes parameters of polarised radiation are denoted $I, Q, U, V \in \mathrm{L}^2(\mathbb{S}^2)$, where $I$ encodes the intensity, $Q$ and $U$ the linear polarisation of the incident radiation, and $V$ the circular polarisation component, which is assumed to be zero. The linear polarisation signal that is observed depends on the choice of local coordinate frame. The component $(Q \pm \mathrm{i}U)$ transforms under a rotation of the local coordinate frame by $\chi \in [0, 2\pi)$ as $(Q \pm \mathrm{i}U)'(\omega) = e^{(\mp \mathrm{i}2\chi)}(Q \pm \mathrm{i}U)(\omega)$ and is thus a spin $\pm 2$ signal on the sphere [45] (hereafter the appropriate spin number subscript is denoted). The quantity $_{\pm 2}(Q \pm \mathrm{i}U)$ can be decomposed into parity even and odd components, so-called E- and B-modes, by

$$\tilde{E}(\omega) = -\frac{1}{2}\left[\bar{\eth}^2\,_2(Q + \mathrm{i}U)(\omega) + \eth^2\,_{-2}(Q - \mathrm{i}U)(\omega)\right] \quad (9)$$

and

$$\tilde{B}(\omega) = \frac{\mathrm{i}}{2}\left[\bar{\eth}^2\,_2(Q + \mathrm{i}U)(\omega) - \eth^2\,_{-2}(Q - \mathrm{i}U)(\omega)\right], \quad (10)$$

respectively, where $\tilde{E}, \tilde{B} \in \mathrm{L}^2(\mathbb{S}^2)$ are scalar signals [45]. The spin spherical harmonic coefficients of the $_{\pm 2}(Q \pm \mathrm{i}U)$ Stokes signal are related to the scalar spherical harmonic coefficients of the E- and B-mode signals by

$$_{\pm 2}(Q \pm \mathrm{i}U)_{\ell m} = -(E_{\ell m} \pm \mathrm{i}B_{\ell m}), \quad (11)$$

where $\tilde{B}_{\ell m} = \sqrt{\frac{(\ell+2)!}{(\ell-2)!}}\, B_{\ell m}$ and $\tilde{E}_{\ell m} = \sqrt{\frac{(\ell+2)!}{(\ell-2)!}}\, E_{\ell m}$.

### C. Signals on the rotation group

Since we construct directional wavelet transforms, we also consider square integrable functions on the rotation group $f \in \mathrm{L}^2(\mathrm{SO}(3))$, where rotations are parameterised by the Euler angles $\rho = (\alpha, \beta, \gamma)$, with $\alpha \in [0, 2\pi)$, $\beta \in [0, \pi]$ and $\gamma \in [0, 2\pi)$. We adopt the *zyz* Euler convention corresponding to the rotation of a physical body in a *fixed* coordinate system about the $z$, $y$ and $z$ axes by $\gamma$, $\beta$ and $\alpha$, respectively.

The Wigner $D$-functions $D_{mn}^{\ell} \in \mathrm{L}^2(\mathrm{SO}(3))$, with natural $\ell \in \mathbb{N}$ and integer $m, n \in \mathbb{Z}$, $|m|, |n| \leq \ell$, are the matrix elements of the irreducible unitary representation of the rotation group $\mathrm{SO}(3)$ [62]. Consequently, the $D_{mn}^{\ell *}$ also form an orthogonal basis in $\mathrm{L}^2(\mathrm{SO}(3))$.[2] The Wigner $D$-functions satisfy the conjugate symmetry relation $D_{mn}^{\ell *}(\rho) = (-1)^{m+n}D_{-m,-n}^{\ell}(\rho)$. The orthogonality and completeness relations for the Wigner $D$-functions read $\langle D_{mn}^{\ell},\ D_{m'n'}^{\ell'}\rangle = 8\pi^2\delta_{\ell\ell'}\delta_{mm'}\delta_{nn'}/(2\ell+1)$ and

$$\sum_{\ell=0}^{\infty}\sum_{m=-\ell}^{\ell}\sum_{n=-\ell}^{\ell} D_{mn}^{\ell}(\alpha, \beta, \gamma)\, D_{mn}^{\ell *}(\alpha', \beta', \gamma')$$
$$= \delta(\alpha - \alpha')\delta(\cos\beta - \cos\beta')\,\delta(\gamma - \gamma'), \quad (12)$$

respectively [62]. The inner product of $f, g \in \mathrm{L}^2(\mathrm{SO}(3))$ is defined by

$$\langle f,\ g\rangle = \int_{\mathrm{SO}(3)} \mathrm{d}\varrho(\rho)\, f(\rho)\, g^*(\rho), \quad (13)$$

where $\mathrm{d}\varrho(\rho) = \sin\beta\,\mathrm{d}\alpha\,\mathrm{d}\beta\,\mathrm{d}\gamma$ is the usual invariant measure on the rotation group. Note that $\langle \cdot,\ \cdot\rangle$ is used to denote inner

[2] We adopt the conjugate $D$-functions as basis elements since this convention simplifies connections to wavelet transforms on the sphere.

products over both the sphere and the rotation group (the case adopted can be inferred from the context). The Wigner $D$-functions may also be related to the spin spherical harmonics by [56]

$$_sY_{\ell m}(\theta, \varphi) = (-1)^s\sqrt{\frac{2\ell+1}{4\pi}}\, D_{m,-s}^{\ell *}(\varphi, \theta, 0). \quad (14)$$

Due to the orthogonality and completeness of the Wigner $D$-functions, any square integrable function on the rotation group $f \in \mathrm{L}^2(\mathrm{SO}(3))$ may be represented by its Wigner expansion

$$f(\rho) = \sum_{\ell=0}^{\infty}\frac{2\ell+1}{8\pi^2}\sum_{m=\ell}^{\ell}\sum_{n=-\ell}^{\ell} f_{mn}^{\ell}D_{mn}^{\ell *}(\rho), \quad (15)$$

where the Wigner coefficients are given by the projection onto each basis function: $f_{mn}^{\ell} = \langle f,\ D_{mn}^{\ell *}\rangle$. The conjugate symmetry relation of the Wigner coefficients is given by $f_{mn}^{\ell *} = (-1)^{m+n}f_{-m,-n}^{\ell}$ for a real function satisfying $f^* = f$ and follows directly from the conjugate symmetry of the Wigner $D$-functions. Throughout, we consider signals on the rotation group band-limited at $L$, that is signals such that $f_{mn}^{\ell} = 0$, $\forall\ell \geq L$. The Wigner transform can be computed exactly and efficiently for band-limited signals by appealing to sampling theorems on the rotation group and fast algorithms [61], [63].

### D. Rotation of signals on the sphere

The rotation of a spin function on the sphere $_sf \in \mathrm{L}^2(\mathbb{S}^2)$ is defined by

$$(\mathcal{R}_{\rho}\,_sf)(\omega) \equiv {}_sf(\mathsf{R}_{\rho}^{-1}\hat{\omega}), \quad (16)$$

where $\hat{\omega}$ denotes the Cartesian vector corresponding to $\omega$ and $\mathsf{R}_{\rho}$ is the three-dimensional rotation matrix corresponding to the rotation operator $\mathcal{R}_{\rho}$. It is convenient to also express the rotation operator in harmonic space.

First, we note the additive property of the Wigner $D$-functions given by [64]

$$D_{mn}^{\ell}(\rho) = \sum_{k=-\ell}^{\ell} D_{mk}^{\ell}(\rho_1)\, D_{kn}^{\ell}(\rho_2), \quad (17)$$

where $\rho$ describes the rotation formed by compositing the rotations described by $\rho_1$ and $\rho_2$, *i.e.* $\mathsf{R}_{\rho} = \mathsf{R}_{\rho_1}\mathsf{R}_{\rho_2}$. By noting the relation between the Wigner $D$-functions and the spin spherical harmonics of Eq. (14), it follows that the spin spherical harmonics can be rotated by

$$(\mathcal{R}_{\rho}\,_sY_{\ell m})(\omega) = \sum_{n=-\ell}^{\ell} D_{nm}^{\ell}(\rho)\,_sY_{\ell n}(\omega), \quad (18)$$

and thus

$$(\mathcal{R}_{\rho}\,_sf)_{\ell m} = \sum_{n=-\ell}^{\ell} D_{mn}^{\ell}(\rho)\,_sf_{\ell n}. \quad (19)$$

## III. DIRECTIONAL SPIN WAVELET TRANSFORM ON THE SPHERE

The directional spin scale-discretised wavelet transform on the sphere is developed in this section. We present the wavelet analysis and synthesis of a signal of arbitrary spin (*i.e.* forward and inverse wavelet transforms), before describing the construction of the wavelets themselves. Important properties of the directional spin wavelet transform are then discussed.

### A. Wavelet analysis

The spin scale-discretised wavelet transform on the sphere of a spin function ${}_s f \in \mathrm{L}^2(\mathbb{S}^2)$ may be defined analogously to the scalar transform, with wavelet coefficients given by the directional convolution

$$W^{{}_s \Psi^{(j)}}(\rho) \equiv ({}_s f \circledast {}_s \Psi^{(j)})(\rho) \equiv \langle {}_s f, \, \mathcal{R}_\rho \, {}_s \Psi^{(j)} \rangle$$
$$= \int_{\mathbb{S}^2} \mathrm{d}\Omega(\omega) \, {}_s f(\omega) \, (\mathcal{R}_\rho \, {}_s \Psi^{(j)})^*(\omega) \,, \quad (20)$$

where the operator $\circledast$ denotes directional convolution on the sphere and the wavelet ${}_s \Psi^{(j)} \in \mathrm{L}^2(\mathbb{S}^2)$ is now also a spin function on the sphere. The wavelets are designed to be localised in scale, position and orientation, and are constructed explicitly in Sec. III-C. The wavelet transform of Eq. (20) thus probes directional structure in the signal of interest ${}_s f$, where $\gamma$ of $\rho = (\alpha, \beta, \gamma)$ can be viewed as the orientation about each point on the sphere $(\theta, \varphi) = (\beta, \alpha)$. The wavelet scale $j \in \mathbb{N}_0$ encodes the angular localisation of $\Psi^{(j)}$.

By decomposing the function ${}_s f$ and wavelet ${}_s \Psi^{(j)}$ into their spherical harmonic expansions, and noting the orthogonality of the spin spherical harmonics and their rotation by Eq. (18), the wavelet transform of Eq. (20) may be written

$$W^{{}_s \Psi^{(j)}}(\rho) = \sum_{\ell=0}^{\infty} \sum_{m=-\ell}^{\ell} \sum_{n=-\ell}^{\ell} {}_s f_{\ell m} \, {}_s \Psi^{(j)*}_{\ell n} \, D^{\ell *}_{mn}(\rho) \,, \quad (21)$$

where ${}_s f_{\ell m} = \langle {}_s f, \, {}_s Y_{\ell m} \rangle$ and ${}_s \Psi^{(j)}_{\ell m} = \langle {}_s \Psi^{(j)}, \, {}_s Y_{\ell m} \rangle$ are the spin spherical harmonic coefficients of the function of interest and wavelet, respectively. Eq. (21) is the spin generalisation of the harmonic representation of the directional convolution typically considered for scalar functions [3], [9], [11], [65], [66]. From Eq. (21) it is apparent that the spin wavelet transform results in scalar wavelet coefficients defined on the rotation group. Comparing Eq. (21) and Eq. (15) it is apparent that the Wigner coefficients of the wavelet coefficients defined on SO(3) are given by

$$\left( W^{{}_s \Psi^{(j)}} \right)^\ell_{mn} = \frac{8\pi^2}{2\ell + 1} \, {}_s f_{\ell m} \, {}_s \Psi^{(j)*}_{\ell n} \,, \quad (22)$$

where $\left( W^{{}_s \Psi^{(j)}} \right)^\ell_{mn} = \langle W^{{}_s \Psi^{(j)}}, \, D^{\ell *}_{mn} \rangle$, as noted previously for the scalar setting [3], [9], [11]. As we elaborate further in Sec. IV-A, the forward wavelet transform of Eq. (20) may thus be computed via an inverse Wigner transform.

The wavelets do not probe the low-frequency content of the signal ${}_s f$; hence, a scaling function ${}_s \Phi \in \mathrm{L}^2(\mathbb{S}^2)$ is introduced for this purpose, with scaling coefficients $W^{{}_s \Phi^{(j)}} \in \mathrm{L}^2(\mathbb{S}^2)$ given by the axisymmetric convolution

$$W^{{}_s \Phi}(\omega) \equiv ({}_s f \odot {}_s \Phi)(\omega) \equiv \langle {}_s f, \, \mathcal{R}_\omega \, {}_s \Phi \rangle \quad (23)$$
$$= \int_{\mathbb{S}^2} \mathrm{d}\Omega(\omega') \, {}_s f(\omega') \, (\mathcal{R}_\omega \, {}_s \Phi)^*(\omega') \,, \quad (24)$$

where we adopt the shorthand notation $\mathcal{R}_\omega = \mathcal{R}_{(\varphi, \theta, 0)}$ and the operator $\odot$ denotes axisymmetric convolution on the sphere with kernels that are invariant under azimuthal rotations when centred on the North pole. We design the scaling function to be axisymmetric such that $\mathcal{R}_{(0,0,\gamma)} {}_s \Phi = {}_s \Phi$ since directional structure of the low-frequency signal content probed by the scaling function is not typically of interest. Consequently, the spin spherical harmonic coefficients of the scaling function are non-zero for $m = 0$ only: ${}_s \Phi_{\ell 0} \delta_{m0} = \langle {}_s \Phi, \, {}_s Y_{\ell m} \rangle$.

It follows from Eq. (21) that the scaling coefficients may be decomposed into their harmonic expansion

$$W^{{}_s \Phi}(\omega) = \sum_{\ell=0}^{\infty} \sum_{m=-\ell}^{\ell} \sqrt{\frac{4\pi}{2\ell + 1}} \, {}_s f_{\ell m} \, {}_s \Phi^*_{\ell 0} \, Y_{\ell m}(\omega) \,, \quad (25)$$

where we have noted Eq. (14). Notice that the scaling coefficients are a scalar function on the sphere, even when analysing a spin function ${}_s f$ (*cf.* the wavelet coefficients). Clearly, the spherical harmonic coefficients of the scaling coefficients read

$$\left( W^{{}_s \Phi} \right)_{\ell m} = \sqrt{\frac{4\pi}{2\ell + 1}} \, {}_s f_{\ell m} \, {}_s \Phi^*_{\ell 0} \,, \quad (26)$$

where $\left( W^{{}_s \Phi} \right)_{\ell m} = \langle W^{{}_s \Phi}, \, Y_{\ell m} \rangle$.

### B. Wavelet synthesis

The signal ${}_s f$ can be synthesised exactly from its wavelet and scaling coefficients by

$$
\begin{aligned}
{}_s f(\omega) = & \int_{\mathbb{S}^2} \mathrm{d}\Omega(\omega') \, W^{{}_s \Phi}(\omega') \, (\mathcal{R}_{\omega'} \, {}_s \Phi)(\omega) \\
& + \sum_{j=J_0}^{J} \int_{\mathrm{SO}(3)} \mathrm{d}\varrho(\rho) \, W^{{}_s \Psi^j}(\rho) \, (\mathcal{R}_\rho \, {}_s \Psi^j)(\omega) \,, \quad (27)
\end{aligned}
$$

where $J_0$ and $J$ are the minimum and maximum wavelet scales considered, respectively, *i.e.* $J_0 \leq j \leq J$, and are defined explicitly in Sec. III-C.

By decomposing the wavelet and scaling coefficients and functions into their harmonic expansions, noting the orthogonality of the spherical harmonics and the Wigner $D$-functions, and also Eq. (14) and Eq. (19), Eq. (27) may be written

$$
\begin{aligned}
{}_s f(\omega) = \sum_{\ell=0}^{\infty} \sum_{m=-\ell}^{\ell} & \left[ \sqrt{\frac{4\pi}{2\ell + 1}} \left( W^{{}_s \Phi} \right)_{\ell m} \, {}_s \Phi_{\ell 0} \right. \\
& \left. + \sum_{j=J_0}^{J} \sum_{n=-\ell}^{\ell} \left( W^{{}_s \Psi^{(j)}} \right)^\ell_{mn} \, {}_s \Psi^{(j)}_{\ell n} \right] {}_s Y_{\ell m}(\omega) \,. \quad (28)
\end{aligned}
$$

As we elaborate further in Sec. IV-A, the inverse wavelet transform of Eq. (27) may thus be computed via a forward Wigner transform. Noting Eq. (22) and Eq. (26), it is clear that ${}_s f$ can only by synthesised from its wavelet and scaling

coefficients through Eq. (27) if the admissibility condition given by the following resolution of the identity holds:

$$\frac{4\pi}{2\ell+1}\big|_s\Phi_{\ell 0}\big|^2 + \frac{8\pi^2}{2\ell+1}\sum_{j=J_0}^{J}\sum_{n=-\ell}^{\ell}\big|_s\Psi_{\ell n}^{(j)}\big|^2 = 1\,, \quad \forall\ell\,. \quad (29)$$

### C. Wavelet construction

We have specified that wavelets should be well-localised in both the spatial and harmonic domains and satisfy the admissibility condition of Eq. (29) but we have not yet defined an explicit construction. We are now in a position to construct wavelets that satisfy these properties. We follow the design of scalar scale-discretised wavelets [9]–[11], [54], which are constructed in harmonic space. However, rather than construct wavelets in the space of scalar spherical harmonics, we construct them in the space of spin spherical harmonics.

Wavelets are defined in spin spherical harmonic space in the factorised form:

$$_s\Psi_{\ell m}^{(j)} \equiv \sqrt{\frac{2\ell+1}{8\pi^2}}\,\kappa^{(j)}(\ell)\,_s\zeta_{\ell m}\,, \quad (30)$$

in order to control their angular and directional localisation separately, respectively through the kernel $\kappa^{(j)} \in \mathrm{L}^2(\mathbb{R}^+)$ and directionality component $_s\zeta \in \mathrm{L}^2(\mathbb{S}^2)$, with harmonic coefficients $_s\zeta_{\ell m} = \langle_s\zeta,\,_sY_{\ell m}\rangle$. Without loss of generality, the directionality component is normalised to impose

$$\sum_{m=-\ell}^{\ell}|_s\zeta_{\ell m}|^2 = 1\,, \quad (31)$$

for all values of $\ell$ for which $\zeta_{\ell m}$ are non-zero for at least one value of $m$. The angular localisation properties of the wavelet $_s\Psi^{(j)}$ are then controlled by the kernel $\kappa^{(j)}$, while the directionality component $\zeta$ controls the directional properties of the wavelet (*i.e.* the behaviour of the wavelet with respect to the azimuthal variable $\varphi$, when centred on the North pole).

The kernel $\kappa^{(j)}(t)$ is a positive real function, with argument $t \in \mathbb{R}^+$, although $\kappa^{(j)}(t)$ is evaluated only at natural arguments $t = \ell$ in Eq. (30). The kernel controls the angular localisation of the wavelet and is constructed to be a smooth function with compact support, as follows. Consider the infinitely differentiable Schwartz function with compact support $t \in [\lambda^{-1}, 1]$, for dilation parameter $\lambda \in \mathbb{R}_*^+$, $\lambda > 1$:

$$s_\lambda(t) \equiv s\left(\frac{2\lambda}{\lambda-1}(t-\lambda^{-1})-1\right)\,, \quad (32)$$

where

$$s(t) \equiv \begin{cases} \exp\big(-(1-t^2)^{-1}\big), & t \in [-1,1] \\ 0, & t \notin [-1,1] \end{cases}\,. \quad (33)$$

Define the smoothly decreasing function $k_\lambda$ by

$$k_\lambda(t) \equiv \frac{\int_t^1 \frac{\mathrm{d}t'}{t'}s_\lambda^2(t')}{\int_{\lambda^{-1}}^1 \frac{\mathrm{d}t'}{t'}s_\lambda^2(t')}, \quad (34)$$

which is unity for $t < \lambda^{-1}$, zero for $t > 1$, and is smoothly decreasing from unity to zero for $t \in [\lambda^{-1}, 1]$. Define the wavelet kernel generating function by

$$\kappa_\lambda(t) \equiv \sqrt{k_\lambda(\lambda^{-1}t)-k_\lambda(t)}\,, \quad (35)$$

which has compact support $t \in [\lambda^{-1}, \lambda]$ and reaches a peak of unity at $t = 1$. The scale-discretised wavelet kernel for scale $j$ is then defined by[3]

$$\kappa^{(j)}(\ell) \equiv \kappa_\lambda(\lambda^{-j}\ell)\,, \quad (36)$$

which has compact support on $\ell \in \big[\lfloor\lambda^{j-1}\rfloor, \lceil\lambda^{j+1}\rceil\big]$, where $\lfloor\cdot\rfloor$ and $\lceil\cdot\rceil$ are the floor and ceiling functions respectively, and reaches a peak of unity at $\lambda^j$.

The directionality component $\zeta$ is constructed to carefully control the directional localisation of the wavelet. An azimuthal band-limit $N$ is imposed such that $\zeta_{\ell m} = 0$, $\forall\ell, m$ with $|m| \geq N$. The directionality component is defined by imposing a specific form for the directional auto-correlation of the wavelet, as outlined in [9], [54] and presented in detail in [54]. The resulting directionality component reads

$$_s\zeta_{\ell m} = \eta\,\upsilon\sqrt{\frac{1}{2^p}\binom{p}{(p-m)/2}}\,, \quad (37)$$

where $\eta = 1$ for $N-1$ odd and $\eta = \mathrm{i}$ for $N-1$ even, $\upsilon = [1-(-1)^{N+m}]/2$ and $p = \min\{N-1, \ell-[1+(-1)^{N+\ell}]/2\}$. We have imposed the symmetries $_s\zeta(\theta, -\varphi) = (-1)^{N-1}\,_s\zeta(\theta,\varphi)$ and $_s\zeta(\theta,\varphi+\pi) = (-1)^{N-1}\,_s\zeta(\theta,\varphi)$.

Scaling functions are required to probe the low-frequency content of the signal of interest not probed by the wavelets and are thus defined by

$$_s\Phi_{\ell m} \equiv \sqrt{\frac{2\ell+1}{4\pi}}\sqrt{k_\lambda(\lambda^{-J_0}\ell)}\,\delta_{m0}\,. \quad (38)$$

The maximum wavelet scale $J$ is set to ensure the wavelets reach the band-limit $L$ of the signal of interest, yielding $J = \lceil\log_\lambda(L-1)\rceil$. The minimum wavelet scale $J_0$ may be freely chosen, provided $0 \leq J_0 < J$. For $J_0 = 0$, the wavelets probe the entire frequency content of the signal of interest except its mean, which is incorporated in the scaling coefficients.

By the construction presented here, the wavelets and scaling functions tile the harmonic line $\ell$, as illustrated in Fig. 1, while satisfying the admissibility condition of Eq. (29). Wavelets are well-localised simultaneously in the spatial domain, both in position and orientation, and the harmonic domain. It is shown in [54] that scale-discretised wavelets exhibit excellent concentration properties, both in the scalar setting and in the spin setting presented in this article. Examples of spin scale-discretised wavelets are plotted in Fig. 2. Notice that the absolute value of the spin scale-discretised wavelets is directional.

### D. Steerability

A function on the sphere is steerable if an azimuthal rotation of the function can be written as a linear combination of weighted basis functions. The steerability property of scalar scale-discretised wavelets extends directly to the spin setting. By imposing an azimuthal band-limit $N$ on the directionality component such that $_s\zeta_{\ell m} = 0$, $\forall\ell, m$ with $|m| \geq N$, we recover wavelets that are steerable [9], [67]. Moreover, if

---

[3]We adopt the $j$ indexing convention followed by [10] where increasing $j$ corresponds to smaller angular scales but higher frequency content, which differs to the convention adopted in [9], [11], [54].
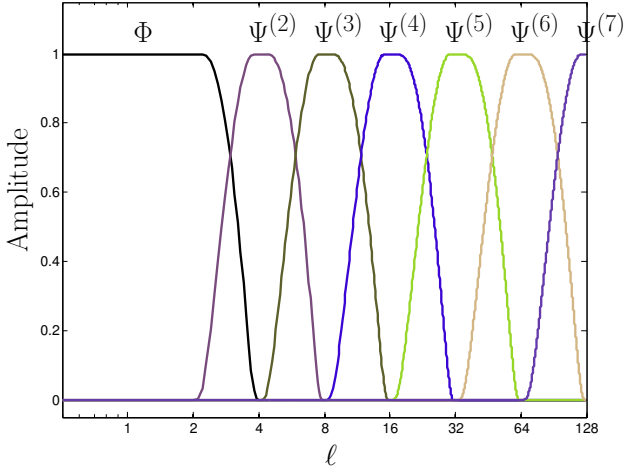
Fig. 1. Scale-discretised wavelet tiling in spin spherical harmonic space ($L = 128$, $\lambda = 2$, $J_0 = 2$, $J = 7$).



(a) Real$\{_2\Psi^{(j=1)}\}$    (b) Imag$\{_2\Psi^{(j=1)}\}$    (c) Abs$\{_2\Psi^{(j=1)}\}$

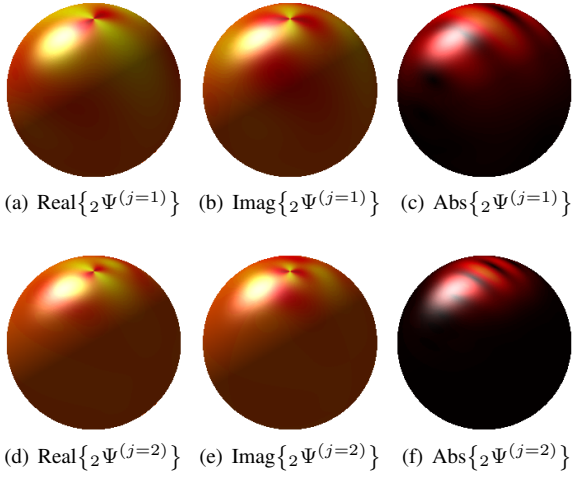(d) Real$\{_2\Psi^{(j=2)}\}$    (e) Imag$\{_2\Psi^{(j=2)}\}$    (f) Abs$\{_2\Psi^{(j=2)}\}$

Fig. 2. Spin scale-discretised wavelets on the sphere ($s = 2$, $\lambda = 2$, $N = 5$). Notice that the absolute value of the wavelet is directional, allowing it to probe signal content localised not only in scale and position but also orientation.

$T \in \mathbb{N}$ of the harmonic coefficients $_s\zeta_{\ell m}$ are non-zero for a given $m$ for at least one $\ell$, then the number of basis functions $M \in \mathbb{N}$ required to steer the wavelet directionality component satisfies $M \geq T$ and the optimal number $M = T$ can be chosen. Furthermore, if $_s\zeta$ exhibits an azimuthal band-limit, then it can be steered using basis functions that are in fact rotations of itself:

$$(\mathcal{R}_{(0,0,\gamma)\,s}\zeta)(\omega) = \sum_{g=0}^{M-1} z(\gamma - \gamma_g) \left( \mathcal{R}_{(0,0,\gamma_g)\,s}\zeta \right)(\omega) \,, \quad (39)$$

where $g \in \mathbb{N}$. The rotation angles $\gamma_g \in [0, 2\pi)$ and interpolating function $z \in \mathrm{L}^2(\mathbb{R})$ are defined subsequently. Note that the interpolating function is independent of the directionality component $_s\zeta$ of the wavelet. Due to the linearity of the wavelet transform, the steerability property is transferred to the wavelet coefficients themselves, yielding

$$W^{s\,\Psi^{(j)}}(\alpha, \beta, \gamma) = \sum_{g=0}^{M-1} z(\gamma - \gamma_g) \, W^{s\,\Psi^{(j)}}(\alpha, \beta, \gamma_g) \,. \quad (40)$$
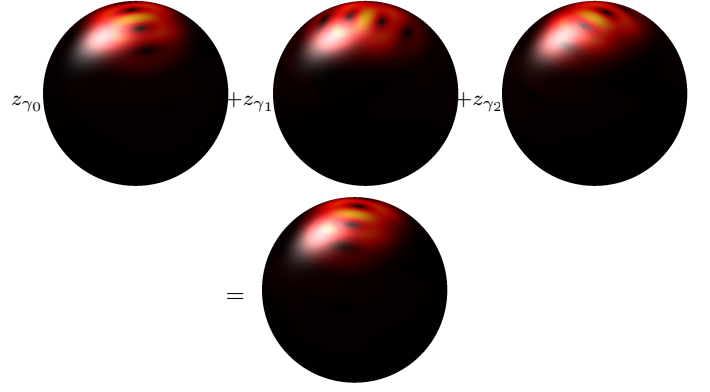


Fig. 3. Absolute value of basis and steered spin wavelets ($s = 2$, $\lambda = 2$, $N = 3$, $j = 3$). The wavelet can be steered to any continuous orientation $\gamma$ by taking weighted sums of its three basis wavelets.

Steerability may be proved, and the interpolating functions defined explicitly, by considering the harmonic expansion of Eq. (39). It follows that the Fourier coefficients of the interpolating function are given by $z_m = 1/M$ and the symmetries of $_s\zeta$ outlined in Sec. III-C may be exploited to optimise the number of basis functions to $M = N$, with equiangular sampling $\gamma_g = g\pi/M$. The derivation is entirely analogous to the scalar setting [9], [54].

A steered wavelet for $N = 3$ and its basis wavelets, given by rotated versions of the wavelet, are plotted in Fig. 3. The wavelet can be steered to any continuous orientation $\gamma$ by taking weighted sums of its three basis wavelets.

*E. Parseval frame*

Spin scale-discretised wavelets on the sphere satisfy the following tight frame property:

$$A \, \|_s f\|^2 \leq \int_{\mathbb{S}^2} \mathrm{d}\Omega(\omega) \left| \langle _s f, \mathcal{R}_\omega \, _s\Phi \rangle \right|^2$$
$$+ \sum_{j=J_0}^{J} \int_{\mathrm{SO}(3)} \mathrm{d}\varrho(\rho) \left| \langle _s f, \mathcal{R}_\rho \, _s\Psi^{(j)} \rangle \right|^2 \leq B \, \|_s f\|^2 \,, \quad (41)$$

with $A = B \in \mathbb{R}_+^*$, for any band-limited $_s f \in \mathrm{L}^2_*(\mathbb{S}^2)$, and where $\| \cdot \|^2 = \langle \cdot, \cdot \rangle$. We adopt a shorthand integral notation in Eq. (41), although by appealing to exact quadrature rules [60], [61] these integrals may be replaced by finite sums.

This property may be proved by considering the term between inequalities in Eq. (41) and substituting harmonic expansions of all terms, such that it reads

$$\sum_{\ell=0}^{\infty} \sum_{m=-\ell}^{\ell} \frac{4\pi}{2\ell+1} |_s f_{\ell m}|^2 |_s\Phi_{\ell 0}|^2$$
$$+ \sum_{j=J_0}^{J} \sum_{\ell=0}^{\infty} \sum_{m=-\ell}^{\ell} \sum_{n=-\ell}^{\ell} \frac{8\pi^2}{2\ell+1} |_s f_{\ell m}|^2 |_s\Psi_{\ell n}^{(j)}|^2 \,, \quad (42)$$

where we have also noted the orthogonality of the spin spherical harmonics and the Wigner $D$-functions. By the wavelet admissibility condition Eq. (29) it follows that Eq. (42) reduces to $\|_s f\|^2$. Spin scale discretised wavelets hence constitute a Parseval frame on the sphere, where $A = B = 1$.

## F. Connection to scalar wavelet transform

For spin $s = \pm 2$ signals, a connection can be made between the spin wavelet transform of $_2(Q + iU)$ and scalar wavelet transforms of E- and B-mode signals, which are not directly observable. First, consider the wavelet coefficients of the observable $_2(Q + iU)$ signal computed by a *spin* wavelet transform: $W^{2\Psi^{(j)}}_{2(Q+iU)}(\rho) \equiv \langle _2(Q + iU), \mathcal{R}_\rho\, _2\Psi^{(j)} \rangle$. Second, consider the wavelet coefficients of the unobservable $\tilde{E}$ and $\tilde{B}$ signals computed by a *scalar* wavelet transform: $W^{0\tilde{\Psi}^j}_{\tilde{E}}(\rho) \equiv \langle \tilde{E}, \mathcal{R}_\rho\, _0\tilde{\Psi}^j \rangle$ and $W^{0\tilde{\Psi}^j}_{\tilde{B}}(\rho) \equiv \langle \tilde{B}, \mathcal{R}_\rho\, _0\tilde{\Psi}^j \rangle$. If the wavelet used in the scalar wavelet transform is a spin lowered version of the wavelet used in the spin wavelet transform, *i.e.* $_0\tilde{\Psi}^j = \bar{\eth}^2\, _2\Psi^j$, then the wavelet coefficients of $\tilde{E}$ and $\tilde{B}$ are simply related to the wavelet coefficients of $_2(Q + iU)$ by $W^{0\tilde{\Psi}^j}_{\tilde{E}}(\rho) = -\mathrm{Re}\big[W^{2\Psi^j}_{2(Q+iU)}(\rho)\big]$ and $W^{0\tilde{\Psi}^j}_{\tilde{B}}(\rho) = -\mathrm{Im}\big[W^{2\Psi^j}_{2(Q+iU)}(\rho)\big]$, respectively. Similar connections for spin-2 signals are shown for standard and mixed needlets [47]–[49]. In a forthcoming article we exploit this property to estimate CMB E- and B-mode maps from $Q$ and $U$ Stokes parameter maps observed in the presence of partial-sky coverage [68].

## IV. EXACT AND EFFICIENT COMPUTATION

The scale-discretised wavelet transform of band-limited spin signals on the sphere can be computed exactly and efficiently by appealing to sampling theorems on the sphere [57], [60] and rotation group [61] and corresponding fast transforms. By exploiting these sampling theorems we develop a new fast algorithm, which is theoretically exact, to compute the scale-discretised wavelet transform to very high band-limits. Moreover, our algorithm requires approximately half as many wavelet coefficients to capture the full information content of band-limited signals compared to alternative approaches [11]. We then discuss and evaluate the numerical implementation of this algorithm.

## A. Fast algorithm

As noted previously, forward and inverse wavelet transforms may be computed via inverse and forward Wigner transforms, respectively. We therefore defer the majority of the computation of the scale-discretised wavelet transform to fast algorithms that we developed recently to compute Wigner transforms [61].

In a recent article [61] we developed a novel sampling theorem for signals defined on the rotation group, such as directional wavelet coefficients, by associating the rotation group with the three-torus through a periodic extension. All of the information content of a band-limited signal can be captured in $4L^3$ samples, reducing the number of required samples by a factor of two compared to other equiangular sampling theorems (*e.g.* [57]). Moreover, we developed fast algorithms to compute Wigner transforms to very high band-limits, which are also theoretically exact. We exploit these developments to compute spin scale-discretised wavelet transforms exactly and efficiently. The efficient nature of our sampling theorem on the rotation group [61] means that only half as many

wavelet coefficients must be computed compared to alternative approaches [11], while still capturing the full information content of the signal under analysis.

The forward wavelet transform of Eq. (20) for a given scale $j$ can be represented by the inverse Wigner transform of Eq. (21), with Wigner coefficients given by Eq. (22). For each scale $j$, the complexity of computing Eq. (22) is $\mathcal{O}(NL^2)$, while the complexity of computing Eq. (21) is reduced from the naive case of $\mathcal{O}(N^2L^4)$ to $\mathcal{O}(NL^3)$ by our fast Wigner transform [61]. Recall that $N$ is the azimuthal band-limit of the wavelet. Scaling coefficients can be computed by Eq. (26) at $\mathcal{O}(L^2)$, followed by an inverse spherical harmonic transform at $\mathcal{O}(L^3)$ by exploiting our novel sampling theorem and corresponding fast spherical harmonic transforms [60]. For a given scale $j$, computing the forward wavelet transform is dominated by the inverse Wigner transform and thus scales as $\mathcal{O}(NL^3)$.

The inverse wavelet transform of Eq. (27) can be computed via forward Wigner transforms. It is apparent from Eq. (28) that the spherical harmonic coefficients of $_sf$ can be recovered by

$$
\begin{aligned}
_sf_{\ell m} = {} & \sqrt{\frac{4\pi}{2\ell+1}}\, \big(W^{s\Phi}\big)_{\ell m}\, _s\Phi_{\ell 0} \\
& + \sum_{j=J_0}^{J}\sum_{n=-\ell}^{\ell} \big(W^{s\Psi^{(j)}}\big)^\ell_{mn}\, _s\Psi^{(j)}_{\ell n}\,. \quad (43)
\end{aligned}
$$

Firstly, Wigner coefficients $\big(W^{s\Psi^{(j)}}\big)^\ell_{mn}$ must be computed by a forward Wigner transform of the wavelet coefficients $W^{s\Psi^{(j)}}(\rho)$. By exploiting our novel sampling theorem on the rotation group and fast Wigner transform, the computation of Wigner coefficients for a given scale $j$ can be reduced from the naive case of $\mathcal{O}(N^2L^4)$ to $\mathcal{O}(NL^3)$ [61]. The contribution to $_sf_{\ell m}$ for a given scale $j$ can then be computed at $\mathcal{O}(NL^2)$. The contribution from the scaling coefficients can be computed at $\mathcal{O}(L^2)$ after a spherical harmonic transform at $\mathcal{O}(L^3)$ by exploiting our fast spherical harmonic transforms [60]. For a given scale $j$, computing the contribution to synthesise the original signal from its wavelet coefficients is dominated by the forward Wigner transform and thus scales as $\mathcal{O}(NL^3)$.

We have so far considered individual wavelet scales only. Naively, when including all $J_{\mathrm{tot}} = J - J_0 + 1$ wavelet scales $j$, both the forward and inverse wavelet transforms scale as $\mathcal{O}(J_{\mathrm{tot}}NL^3)$. However, since the wavelets themselves have compact support (see Fig. 1) it is not necessary to perform all wavelet transforms at the full band-limit $L$. Furthermore, the lower support of the wavelets can also be exploited to increase computational efficiency. A multi-resolution algorithm is constructed following these optimisations, where the computation is dominated by the largest two scales. Hence, the overall complexity of computing both forward and inverse wavelet transforms, including all scales, is effectively $\mathcal{O}(NL^3)$. In addition, for real signals we exploit their conjugate symmetry to further reduce computational and memory requirements by a factor of two.

## B. Implementation

We have implemented the exact and efficient algorithm described previously to compute spin scale-discretised wavelet transforms on the sphere in the existing S2LET code [10], which has also been extended to support directional wavelets. The core algorithms of S2LET are implemented in C, while Matlab, Python and IDL interfaces are also provided. Consequently, S2LET is able to handle very large harmonic band-limits, corresponding to data-sets containing tens of millions of pixels. S2LET[4] is publicly available, and relies on the SSHT[5] code [60] to compute spherical harmonic transforms, the SO3[6] code [61] to compute Wigner transforms and the FFTW[7] code to compute Fourier transforms. Note that it also supports the analysis of data on the sphere defined in the common HEALPIX[8] [51] format.

## C. Numerical evaluation

We evaluate the numerical accuracy and computation time of the spin scale-discretised wavelet transform implemented in the S2LET code. We simulate band-limited test signals on the sphere defined by uniformly random spherical harmonic coefficients $_sf_{\ell m}$ with real and imaginary parts distributed in the interval $[-1, 1]$. We then compute an inverse spherical harmonic transform to recover a band-limited test signal on the sphere. A forward wavelet transform is then performed, followed by an inverse transform to synthesise the original signal from its wavelet coefficients. Ten simulated signals are considered for band-limits from $L = 32$ to $L = 2048$. All numerical experiments are performed on a standard desktop with a 3.5 GHz Intel Core i7 processor and 32 GB of RAM.

*1) Numerical accuracy:* Numerical accuracy of a round-trip wavelet transform is measured by the maximum absolute error between the spherical harmonic coefficients of the original test signal $_sf^o_{\ell m}$ and the recomputed values $_sf^r_{\ell m}$, *i.e.* $\epsilon = \max_{\ell, m} |_sf^r_{\ell m} - _sf^o_{\ell m}|$. Results of the numerical accuracy tests, averaged over ten random test signals, are plotted in Fig. 4. We plot results for a spin $s = 2$ signal, although the accuracy for different spin numbers is identical. The numerical accuracy of the round-trip transform is close to machine precision and found empirically to scale as $\mathcal{O}(L)$.

*2) Computation time:* Computation time is measured by the round-trip computation time taken to perform a forward and inverse wavelet transform. Results of the computation time tests, averaged over ten random test signals, are plotted in Fig. 5. We plot results for a spin $s = 2$ signal, although the computation time for different spin numbers is identical since the spin number is simply a parameter of the transform (rather than applied through spin lowering/raising operators). For constant $N$, computation time is found empirically to scale as $\mathcal{O}(L^3)$, as predicted in Sec. IV-A.
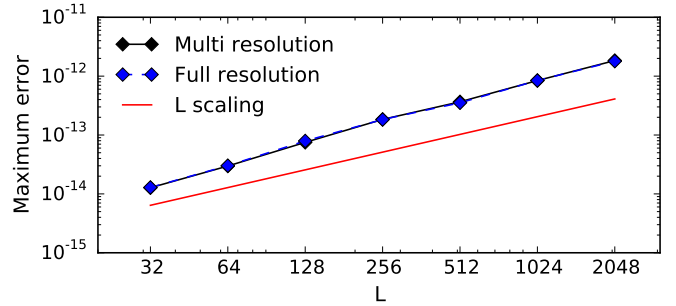
Fig. 4. Numerical accuracy of a round-trip wavelet transform ($s = 2$, $N = 5$, $\lambda = 2$). Accuracy is close to machine precision and found empirically to scale as $\mathcal{O}(L)$.
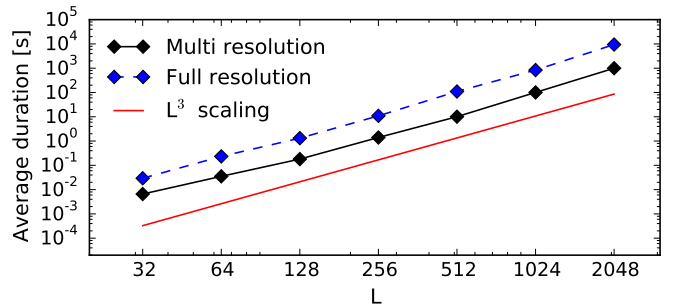


Fig. 5. Computation time of a round-trip wavelet transform ($s = 2$, $N = 5$, $\lambda = 2$). For constant $N$, computation time is found empirically to scale as $\mathcal{O}(L^3)$, as expected. Furthermore, the multiresolution transform is approximately an order of magnitude faster than the full-resolution transform.

## V. ILLUSTRATION

We illustrate the use of spin scale-discretised wavelets in a very simple denoising example. We consider linearly polarised radiation and construct the spin-2 signal $x = _2(Q + iU) \in L^2(\mathbb{S}^2)$ from the $Q$ and $U$ Stokes parameters, as described in Sec. II-B. The observed signal $y \in L^2(\mathbb{S}^2)$ is contaminated with zero-mean Gaussian white noise on the sphere $n \in L^2(\mathbb{S}^2)$, with variance

$$\mathbb{E}(|n_{\ell m}|^2) = \sigma^2, \quad \forall \ell, m, \tag{44}$$

and thus reads $y = x + n$, where all signals are band-limited at $L$.

To assess the fidelity of noisy signals, we consider the signal-to-noise ratio (SNR) defined by

$$\text{SNR}(y) \equiv 10 \log_{10} \frac{\|x\|_2^2}{\|y - x\|_2^2}, \tag{45}$$

where signal energies are calculated by

$$\|x\|_2^2 \equiv \langle x, \, x \rangle = \int_{\mathbb{S}^2} d\Omega(\omega)|x(\omega)|^2 = \sum_{\ell=0}^{L-1} \sum_{m=-\ell}^{\ell} |x_{\ell m}|^2. \tag{46}$$

We estimate $x$ by denoising $y$, to recover the denoised signal $\hat{x} \in L^2(S^2)$, taking advantage of the fact that most natural signals of interest (*e.g.*, generated by physical processes) have their energy concentrated in a small number of wavelet coefficients. By contrast, the energy of the noise is spread over

all wavelet scales. Since the wavelet transform is linear, the wavelet coefficients of the observed signal for the $j$-th scale are simply given by the sum of signal and noise contributions:

$$Y^{^2\Psi^{(j)}}(\rho) = X^{^2\Psi^{(j)}}(\rho) + N^{^2\Psi^{(j)}}(\rho), \qquad (47)$$

where upper-case variables denote wavelet coefficients of the corresponding signal denoted by lower-case variables, *i.e.* $Y^{^2\Psi^{(j)}} \equiv y \circledast {}_2\Psi^{(j)}$. Due, again, to the linearity of the wavelet transform, the wavelet coefficients of the noise are also zero-mean and Gaussian, with variance

$$\mathbb{E}\big(|N^{^2\Psi^{(j)}}(\rho)|^2\big) = \int_{SO(3)} d\varrho(\rho)\big|N^{^2\Psi^{(j)}}(\rho)\big|^2 \qquad (48)$$

$$= \sigma^2 \sum_{\ell n} \big|_2\Psi^{(j)}_{\ell n}\big|^2 \equiv \big(\sigma^{(j)}\big)^2. \qquad (49)$$

Thus, a simple denoising strategy is to hard-threshold the wavelet coefficients $Y^{^2\Psi^{(j)}}$ with a threshold $t^{(j)} = 3\sigma^{(j)}$. This yields denoised wavelet coefficients

$$\hat{X}^{^2\Psi^{(j)}}(\rho) = \begin{cases} 0, & \text{if } Y^{^2\Psi^{(j)}}(\rho) < t^{(j)} \\ Y^{^2\Psi^{(j)}}(\rho), & \text{otherwise} \end{cases} . \qquad (50)$$

Scaling coefficients are not thresholded: we simply take $\hat{X}^{^2\Phi} = Y^{^2\Phi}$. The denoised signal $\hat{x}$ is then reconstructed from its wavelet coefficients $\hat{X}^{^2\Psi^{(j)}}$ and scaling coefficients $\hat{X}^{^2\Phi}$ by an inverse spin wavelet transform.

This simple denoising strategy is demonstrated using the full-sky polarised synchrotron emission that is inferred from WMAP data [69] and shown in Fig. 6, which is used as the input test signal $x$. This test signal is highly structured and generated by real astrophysical processes. Consequently, it is a good example signal for a denoising illustration, even though it already contains some noise. The test signal is corrupted with noise to yield the observed signal $y$, such that $\text{SNR}(y) = 11$ dB. By applying the denoising algorithm described above (with parameters $L = 512$, $\lambda = 2$, $N = 4$, and $J_0 = 0$) a denoised signal $\hat{x}$ is recovered with $\text{SNR}(d) = 18$ dB. Noisy and denoised data are plotted in Fig. 7. Repeating the denoising using axisymmetric spin scale-discretised wavelets (by setting $N = 1$) degrades the fidelity of the denoised signal by $\sim 1$dB. In this illustration, where a very simple hard-thresholding algorithm is adopted, the denoising is surprisingly effective given that the input signal is taken from real astrophysical data and already contains residual noise.

## VI. CONCLUSIONS

The directional spin scale-discretised wavelet framework constructed in this article is the only wavelet framework defined natively on the sphere that is able to probe the directional intensity of spin signals. The wavelet transform can thus be used to probe signal content not only in scale and location but also orientation. This additional degree of freedom improves the sensitivity of wavelet analyses in practical applications, as demonstrated already for scalar signals in numerous analyses of the temperature anisotropies of the CMB (*e.g.* [19]–[21], [24], [25]). In addition, our directional spin scale-discretised wavelet framework supports the exact synthesis of a signal
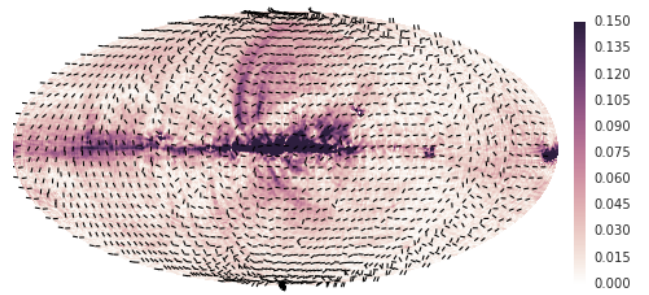


Fig. 6. Full-sky polarised synchrotron emission inferred from WMAP data [69], plotted using a Mollweide projection, in units of $\mu$K. The colour scale of the plot shows the amplitude of the spin-2 signal ${}_2(Q + iU)$, while the direction of the headless vectors show its phase. These data provide the test signal used for the denoising illustration.



(a) $|_2(Q + iU)|$
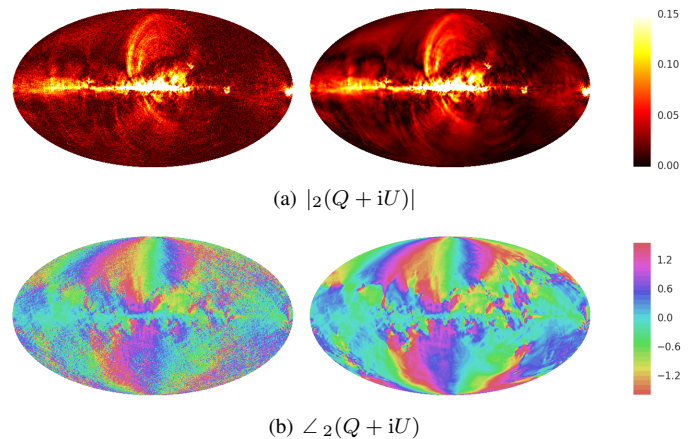


(b) $\angle {}_2(Q + iU)$

Fig. 7. Wavelet denoising of the full-sky polarised synchrotron emission shown in Fig. 6. The amplitude of the spin-2 signal ${}_2(Q + iU)$ is shown in panel (a) in units of $\mu$K, while its phase is shown in panel (b). Noisy data is plotted on the left and denoised data recovered by a simple hard-thresholding strategy is plotted on the right. Noisy data is constructed with an SNR of 11 dB, while denoised data is recovered with an SNR of 18 dB.

from its wavelet coefficients, in theory and in practice, and is applicable to signals of arbitrary spin, while the wavelets themselves constitute a Parseval frame and are steerable, implying wavelet coefficients for any continuous orientation can be computed from a finite number of fixed orientations. Furthermore, we present exact and efficient algorithms to compute the forward and inverse wavelet transform for very large data-sets containing tens of millions of samples on the sphere. We require only half as many wavelet coefficients to capture the full information content of the signal compared to alternative approaches. Finally, we highlight the applicability of spin directional wavelets by a simple illustration of an application to denoising linearly polarised radiation observed on the celestial sphere, which is a spin $s = \pm 2$ signal.

## REFERENCES

[1] J.-P. Antoine and P. Vandergheynst, "Wavelets on the 2-sphere: a group theoretical approach," *Applied Comput. Harm. Anal.*, vol. 7, pp. 1–30, 1999.

[2] ——, "Wavelets on the n-sphere and related manifolds," *J. Math. Phys.*, vol. 39, no. 8, pp. 3987–4008, 1998.

[3] Y. Wiaux, L. Jacques, and P. Vandergheynst, "Correspondence principle between spherical and Euclidean wavelets," *Astrophys. J.*, vol. 632, pp. 15–28, 2005.

[4] J. D. McEwen and A. M. M. Scaife, "Simulating full-sky interferometric observations," *Mon. Not. Roy. Astron. Soc.*, vol. 389, no. 3, pp. 1163–1178, 2008.

[5] J. D. McEwen, Y. Wiaux, and D. M. Eyers, "Data compression on the sphere," *Astron. & Astrophys.*, vol. 531, p. A98, 2011.

[6] F. J. Narcowich, P. Petrushev, and J. D. Ward, "Localized tight frames on spheres," *SIAM J. Math. Anal.*, vol. 38, no. 2, pp. 574–594, 2006.

[7] P. Baldi, G. Kerkyacharian, D. Marinucci, and D. Picard, "Asymptotics for spherical needlets," *Ann. Stat.*, vol. 37 No.3, pp. 1150–1171, 2009.

[8] D. Marinucci, D. Pietrobon, A. Balbi, P. Baldi, P. Cabella, G. Kerkyacharian, P. Natoli, D. Picard, and N. Vittorio, "Spherical needlets for cosmic microwave background data analysis," *Mon. Not. Roy. Astron. Soc.*, vol. 383, pp. 539–545, 2008.

[9] Y. Wiaux, J. D. McEwen, P. Vandergheynst, and O. Blanc, "Exact reconstruction with directional wavelets on the sphere," *Mon. Not. Roy. Astron. Soc.*, vol. 388, no. 2, pp. 770–788, 2008.

[10] B. Leistedt, J. D. McEwen, P. Vandergheynst, and Y. Wiaux, "S2LET: A code to perform fast wavelet analysis on the sphere," *Astron. & Astrophys.*, vol. 558, no. A128, pp. 1–9, 2013.

[11] J. D. McEwen, P. Vandergheynst, and Y. Wiaux, "On the computation of directional scale-discretized wavelet transforms on the sphere," in *SPIE Wavelets and Sparsity XV*, 2013.

[12] J. L. Sanz, D. Herranz, M. López-Caniego, and F. Argüeso, "Wavelets on the sphere – application to the detection problem," in *EUSIPCO*, Sept. 2006.

[13] J. D. McEwen, M. P. Hobson, and A. N. Lasenby, "A directional continuous wavelet transform on the sphere," *ArXiv*, 2006.

[14] J.-L. Starck, Y. Moudden, P. Abrial, and M. Nguyen, "Wavelets, ridgelets and curvelets on the sphere," *Astron. & Astrophys.*, vol. 446, pp. 1191–1204, Feb. 2006.

[15] P. Audet, "Directional wavelet analysis on the sphere: Application to gravity and topography of the terrestrial planets," *J. Geophys. Res.*, vol. 116, no. E1, 2011.

[16] ——, "Toward mapping the effective elastic thickness of planetary lithospheres from a spherical wavelet analysis of gravity and topography," *Phys. Earth Planet In.*, vol. 226, no. 0, pp. 48–82, 2014.

[17] F. J. Simons, I. Loris, G. Nolet, I. C. Daubechies, S. Voronin, J. S. Judd, P. A. Vetter, J. Charléty, and C. Vonesch, "Solving or resolving global tomographic models with spherical wavelets, and the scale and sparsity of seismic heterogeneity," *Geophysical Journal International*, vol. 187, pp. 969–988, Nov. 2011.

[18] P. Vielva, E. Martínez-González, R. B. Barreiro, J. L. Sanz, and L. Cayón, "Detection of non-Gaussianity in the WMAP 1-year data using spherical wavelets," *Astrophys. J.*, vol. 609, pp. 22–34, 2004.

[19] J. D. McEwen, M. P. Hobson, A. N. Lasenby, and D. J. Mortlock, "A high-significance detection of non-Gaussianity in the WMAP 1-year data using directional spherical wavelets," *Mon. Not. Roy. Astron. Soc.*, vol. 359, pp. 1583–1596, 2005.

[20] ——, "A high-significance detection of non-Gaussianity in the WMAP 3-year data using directional spherical wavelets," *Mon. Not. Roy. Astron. Soc.*, vol. 371, pp. L50–L54, 2006.

[21] ——, "A high-significance detection of non-Gaussianity in the WMAP 5-year data using directional spherical wavelets," *Mon. Not. Roy. Astron. Soc.*, vol. 388, no. 2, pp. 659–662, 2008.

[22] ——, "Non-Gaussianity detections in the Bianchi VII$_h$ corrected WMAP 1-year data made with directional spherical wavelets," *Mon. Not. Roy. Astron. Soc.*, vol. 369, pp. 1858–1868, 2006.

[23] P. Vielva, E. Martínez-González, and M. Tucci, "Cross-correlation of the cosmic microwave background and radio galaxies in real, harmonic and wavelet spaces: detection of the integrated Sachs-Wolfe effect and dark energy constraints," *Mon. Not. Roy. Astron. Soc.*, vol. 365, pp. 891–901, 2006.

[24] J. D. McEwen, P. Vielva, M. P. Hobson, E. Martínez-González, and A. N. Lasenby, "Detection of the ISW effect and corresponding dark energy constraints made with directional spherical wavelets," *Mon. Not. Roy. Astron. Soc.*, vol. 373, pp. 1211–1226, 2007.

[25] J. D. McEwen, Y. Wiaux, M. P. Hobson, P. Vandergheynst, and A. N. Lasenby, "Probing dark energy with steerable wavelets through correlation of WMAP and NVSS local morphological measures," *Mon. Not. Roy. Astron. Soc.*, vol. 384, no. 4, pp. 1289–1300, 2008.

[26] P. Vielva, Y. Wiaux, E. Martínez-González, and P. Vandergheynst, "Steerable wavelet analysis of CMB structures alignment," *New Astronomy Review*, vol. 50, pp. 880–888, 2006.

[27] Y. Wiaux, P. Vielva, R. B. Barreiro, E. Martínez-González, and P. Vandergheynst, "Non-Gaussianity analysis on local morphological measures of WMAP data," *Mon. Not. Roy. Astron. Soc.*, vol. 385, pp. 939–947, Apr. 2008.

[28] Y. Wiaux, P. Vielva, E. Martínez-González, and P. Vandergheynst, "Global universe anisotropy probed by the alignment of structures in the cosmic microwave background," *Phys. Rev. Lett.*, vol. 96, p. 151303, 2006.

[29] X. Lan and D. Marinucci, "The needlets bispectrum," *Electronic Journal of Statistics*, vol. 2, pp. 332–367, 2008.

[30] D. Pietrobon, A. Balbi, and D. Marinucci, "Integrated Sachs-Wolfe effect from the cross-correlation of WMAP 3-year and NVSS: new results and constraints on dark energy," *Phys. Rev. D.*, vol. 74, no. 4, pp. 043 524–+, Aug. 2006.

[31] Planck Collaboration XII, "*Planck 2013* results. XII. Diffuse component separation," *Astron. & Astrophys.*, vol. 571, p. A12, 2014.

[32] Planck Collaboration XXIII, "*Planck* 2013 results. XXIII. Isotropy and statistics of the CMB," *Astron. & Astrophys.*, vol. 571, no. A23, 2014.

[33] Planck Collaboration XXV, "*Planck* 2013 results. XXV. Searches for cosmic strings and other topological defects," *Astron. & Astrophys.*, vol. 571, no. A25, 2014.

[34] J. Schmitt, J. L. Starck, J. M. Casandjian, J. Fadili, and I. Grenier, "Poisson denoising on the sphere: application to the Fermi gamma ray space telescope," *Astron. & Astrophys.*, vol. 517, p. A26, July 2010.

[35] J. Bobin, J.-L. Starck, F. Sureau, and S. Basak, "Sparse component separation for accurate cosmic microwave background estimation," *Astron. & Astrophys.*, vol. 550, p. A73, Feb. 2013.

[36] J. Delabrouille, J.-F. Cardoso, M. Le Jeune, M. Betoule, G. Fay, and F. Guilloux, "A full sky, low foreground, high resolution CMB map from WMAP," *Astron. & Astrophys.*, vol. 493, pp. 835–857, Jan. 2009.

[37] J. D. McEwen, P. Vielva, Y. Wiaux., R. B. Barreiro, L. Cayón, M. P. Hobson, A. N. Lasenby, E. Martínez-González, and J. L. Sanz, "Cosmological applications of a wavelet analysis on the sphere," *J. Fourier Anal. and Appl.*, vol. 13, no. 4, pp. 495–510, 2007.

[38] C. Durastanti, Y. Fantaye, F. Hansen, D. Marinucci, and I. Z. Pesenson, "Simple proposal for radial 3D needlets," *Phys. Rev. D.*, vol. 90, no. 10, p. 103532, Nov. 2014.

[39] B. Leistedt and J. D. McEwen, "Exact wavelets on the ball," *IEEE Trans. Sig. Proc.*, vol. 60, no. 12, pp. 6257–6269, 2012.

[40] J. D. McEwen and B. Leistedt, "Fourier-Laguerre transform, convolution and wavelets on the ball," in *10th International Conference on Sampling Theory and Applications (SampTA)*, 2013, pp. 329–333.

[41] F. Lanusse, A. Rassat, and J.-L. Starck, "Spherical 3D isotropic wavelets," *Astron. & Astrophys.*, vol. 540, p. A92, Apr. 2012.

[42] C. P. Ahn, R. Alexandroff, C. Allende Prieto, S. F. Anderson, T. Anderton, B. H. Andrews, É. Aubourg, S. Bailey, E. Balbinot, R. Barnes, and et al., "The Ninth Data Release of the Sloan Digital Sky Survey: First Spectroscopic Data from the SDSS-III Baryon Oscillation Spectroscopic Survey," *Astrophys. J. Supp.*, vol. 203, p. 21, Dec. 2012.

[43] E. T. Newman and R. Penrose, "Note on the Bondi-Metzner-Sachs group," *J. Math. Phys.*, vol. 7, no. 5, pp. 863–870, 1966.

[44] A. Plattner and F. J. Simons, "A spatiospectral localization approach for analyzing and representing vector-valued functions on spherical surfaces," in *SPIE Wavelets and Sparsity XV*, vol. 8858, 2013.

[45] M. Zaldarriaga and U. Seljak, "All-sky analysis of polarization in the microwave background," *Phys. Rev. D.*, vol. 55, no. 4, pp. 1830–1840, Feb 1997.

[46] J. Starck, Y. Moudden, and J. Bobin, "Polarized wavelets and curvelets on the sphere," *Astron. & Astrophys.*, vol. 497, pp. 931–943, Apr. 2009.

[47] D. Geller, F. K. Hansen, D. Marinucci, G. Kerkyacharian, and D. Picard, "Spin needlets for cosmic microwave background polarization data analysis," *Phys. Rev. D.*, vol. 78, no. 12, pp. 123 533–+, 2008.

[48] D. Geller and D. Marinucci, "Spin Wavelets on the Sphere," *J. Fourier Anal. and Appl.*, vol. 16, no. 6, pp. 840–884, Nov. 2010.

[49] ——, "Mixed Needlets," *J. Math. Anal. Appl.*, vol. 375, no. 2, pp. 610–630, June 2011.

[50] D. Geller, X. Lan, and D. Marinucci, "Spin Needlets Spectral Estimation," *Electron. J. Statist.*, vol. 3, pp. 1497–1530, July 2009.

[51] K. M. Górski, E. Hivon, A. J. Banday, B. D. Wandelt, F. K. Hansen, M. Reinecke, and M. Bartelmann, "Healpix – a framework for high resolution discretisation and fast analysis of data distributed on the sphere," *Astrophys. J.*, vol. 622, pp. 759–771, 2005.

[52] J. D. McEwen, "Ridgelet transform on the sphere," *in prep.*, 2015.

[53] Y. Chan, J. D. McEwen, and Others, "Second-generation curvelets on the sphere," *in prep.*, 2015.

[54] J. D. McEwen, C. Durastanti, and Y. Wiaux, "Localisation of directional scale-discretised wavelets on the sphere," *Applied Comput. Harm. Anal.*, submitted, 2015.

[55] J. D. McEwen, M. Büttner, B. Leistedt, H. V. Peiris, P. Vandergheynst, and Y. Wiaux, "On spin scale-discretised wavelets on the sphere for the

analysis of CMB polarisation," in *Proceedings IAU Symposium No. 306, 2014*, 2014.

[56] J. N. Goldberg, A. J. Macfarlane, E. T. Newman, F. Rohrlich, and E. C. G. Sudarshan, "Spin-*s* spherical harmonics and ð," *J. Math. Phys.*, vol. 8, no. 11, pp. 2155–2161, 1967.

[57] J. R. Driscoll and D. M. J. Healy, "Computing Fourier transforms and convolutions on the sphere," *Adv. Appl. Math.*, vol. 15, pp. 202–250, 1994.

[58] Y. Wiaux, L. Jacques, and P. Vandergheynst, "Fast spin $\pm 2$ spherical harmonics transforms," *J. Comput. Phys.*, vol. 226, p. 2359, 2005.

[59] J. D. McEwen, "Fast, exact (but unstable) spin spherical harmonic transforms," *All Res. J. Phys.*, vol. 1, no. 1, 2011.

[60] J. D. McEwen and Y. Wiaux, "A novel sampling theorem on the sphere," *IEEE Trans. Sig. Proc.*, vol. 59, no. 12, pp. 5876–5887, 2011.

[61] J. D. McEwen, M. Büttner, B. Leistedt, H. V. Peiris, and Y. Wiaux, "A novel sampling theorem on the rotation group," *IEEE Sig. Proc. Let., submitted*, 2015.

[62] D. A. Varshalovich, A. N. Moskalev, and V. K. Khersonskii, *Quantum theory of angular momentum*. Singapore: World Scientific, 1989.

[63] P. Kostelec and D. Rockmore, "FFTs on the rotation group," *J. Fourier Anal. and Appl.*, vol. 14, pp. 145–179, 2008.

[64] D. Marinucci and G. Peccati, *Random Fields on the Sphere: Representation, Limit Theorem and Cosmological Applications*. Cambridge University Press, 2011.

[65] J. D. McEwen, M. P. Hobson, D. J. Mortlock, and A. N. Lasenby, "Fast directional continuous spherical wavelet transform algorithms," *IEEE Trans. Sig. Proc.*, vol. 55, no. 2, pp. 520–529, 2007.

[66] Y. Wiaux, L. Jacques, P. Vielva, and P. Vandergheynst, "Fast directional correlation on the sphere with steerable filters," *Astrophys. J.*, vol. 652, pp. 820–832, 2006.

[67] W. Freeman and E. Adelson, "The design and use of steerable filters," *IEEE Trans. Pattern Anal.*, vol. 13, no. 9, pp. 891–906, 1991.

[68] B. Leistedt and Others, "Estimating CMB E- and B-modes with directional spin wavelets," *in prep.*, 2015.

[69] B. Gold, C. L. Bennett, R. S. Hill, G. Hinshaw, N. Odegard, L. Page, D. N. Spergel, J. L. Weiland, J. Dunkley, M. Halpern, N. Jarosik, A. Kogut, E. Komatsu, D. Larson, S. S. Meyer, M. R. Nolta, E. Wollack, and E. L. Wright, "Five-Year Wilkinson Microwave Anisotropy Probe Observations: Galactic Foreground Emission," *Astrophys. J. Supp.*, vol. 180, pp. 265–282, Feb. 2009.